Journal of Solid State Chemistry **167,** 145–151 (2002)
doi:10.1006/jssc.2002.9636

Synthesis and Characterization of the Reduced Single-Layer Manganite $Sr_2MnO_{3.5+x}$

L. J. Gillie,* A. J. Wright,* J. Hadermann,† G. Van Tendeloo,† and C. Greaves*,[1]

*School of Chemical Sciences, University of Birmingham, Birmingham B15 2TT, United Kingdom; and †EMAT, RUCA, Groenenborgerlaan 171, 2020 Antwerp, Belgium

Received December 26, 2001; in revised form April 23, 2002; accepted May 3, 2002

The nuclear and magnetic structures of polycrystalline $Sr_2MnO_{3.5}$ have been determined by the Rietveld analysis of neutron powder diffraction data and electron diffraction techniques. The pure Mn^{3+} single-layered phase crystallizes in the primitive monoclinic space-group $P2_1/c$ with lattice constants $a = 6.8524(3)$ Å; $b = 10.8131(4)$ Å; $c = 10.8068(4)$ Å; $\beta = 113.247(4)^\circ$. The oxygen defects form an ordered superstructure within the perovskite block layers consisting of interconnected MnO_5 square pyramids, slightly different from those observed for the defect perovskites $SrMnO_{2.5}$ and $Ca_2MnO_{3.5}$. Magnetic susceptibility studies show a broad transition at ~ 280 K, which is attributed to an overall antiferromagnetic ordering of spins, which leads to doubling of the unit cell along [100]. The magnetic unit cell comprises ferromagnetic clusters of four corner-sharing MnO_5 pyramids, which are antiferromagnetically aligned to other similar clusters within the perovskite block layers.

Key Words: **strontium manganite, oxygen deficient; strontium manganese oxide; $Sr_2MnO_{3.5}$, magnetic structure; $Sr_2MnO_{3.5}$, neutron diffraction; layered manganese oxide.**

INTRODUCTION

Perovskites containing Mn in mixed Mn^{3+}/Mn^{4+} oxidation states have been the focus of much attention owing to their ability to display large negative magnetoresistance effects upon application of magnetic fields of the order of several tesla (1). In recent years, however, increasing research efforts have been concentrated on low-dimensional structural variants, following the discovery of similar magnetotransport effects in $La_{1.2}Sr_{1.8}Mn_2O_7$ and related phases, but in significantly smaller fields of <1 T (2, 3). $La_{1.2}Sr_{1.8}Mn_2O_7$ is an $n = 2$ member of the Ruddlesden–Popper (RP) (4) class of layered perovskites, which provides a variety of possibilities for low-dimensional manganese materials. We are exploring the possibilities for synthesizing $n = 1$ phases of the type $Sr_2MnO_{4-x}F_x$, which would cover Mn oxidation states from Mn^{3+} ($x = 1$) to Mn^{4+} ($x = 0$). We, therefore, considered a synthetic strategy involving the initial synthesis of the oxygen-deficient Mn^{3+} phase $Sr_2MnO_{3.5}$, with the intention of subsequently using controlled fluorine insertion reactions to achieve oxidation states between Mn^{3+} and $Mn^{3.5+}$.

The oxygenated phase Sr_2MnO_4 has a body-centered tetragonal structure and has been studied extensively to date (5,6). Kriegel *et al.* (7) and Kriegel and Feltz (8) have produced a reduced phase $Sr_2MnO_{3.84(\pm 0.05)}$ which is reported to contain the oxygen vacancies in the "MnO_2" layers (equatorial positions) in a disordered array. The magnetic structure of Sr_2MnO_4, as reported by Bouloux *et al.* (9), is analogous to that of K_2NiF_4. The magnetic unit-cell shows a doubling along the *a*-axis, with the magnetic moments parallel to the *c*-axis exhibiting antiferromagnetic (AFM) ordering with $T_N = 170$ K. This contrasts with the magnetic structure of Ca_2MnO_4 (10) where the *c*-axis was doubled for the magnetic cell. A related double-layered oxygen-deficient strontium manganite, $Sr_3Mn_2O_{6.55}$ has been reported by Mitchell *et al.* (11). This Ruddlesden–Popper structure also has the oxygen defects located in the equatorial "MnO_2" layers, but again, similar to $Sr_2MnO_{3.84}$, these vacancies are found to exist in a disordered manner.

The synthesis of $Ca_2MnO_{3.5}$ has been reported by Leonowicz *et al.* (12) and its defect structure has been studied by neutron diffraction. The phase crystallizes with orthorhombic symmetry in the space group *Bbcm* with lattice parameters, $a = 5.30$ Å; $b = 10.05$ Å; $c = 12.23$ Å. The oxygen vacancies form an ordered arrangement in the perovskite block layers to give an equivalent structure to the defect perovskites $SrMnO_{2.5}$ (13, 14) and $CaMnO_{2.5}$ (15) consisting of corner connected MnO_5 square-based pyramids. In these isostructural phases, the manganese ions

[1]To whom correspondence should be addressed. Fax: +44-121-414-4442. E-mail: c.greaves@bham.ac.uk.

0022-4596/02 $35.00

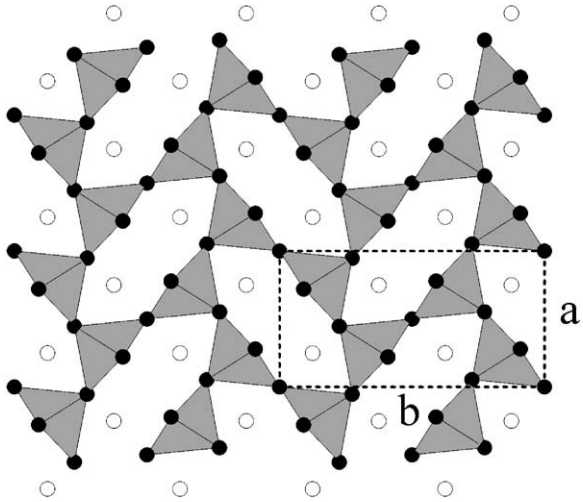

FIG. 1. Defect structure of $SrMnO_{2.5}$ (Gray polyhedra represent MnO_5 square-based pyramids; black spheres represent oxygen anions; white spheres represent strontium ions).

are in square pyramidal co-ordination, and are subject to AFM coupling with three neighboring Mn^{3+} ions, and ferromagnetic (FM) coupling with two others. Figure 1 shows the crystallographic structure of $SrMnO_{2.5}$. In this paper, we show that the structure of $Sr_2MnO_{3.5}$ contains Mn–O layers with a different ordering pattern to that reported previously for layers with the same overall composition, $MnO_{1.5}$. As a result of the different packing of the square pyramidal MnO_5 units, a new magnetic structure is formed below the Néel temperature.

EXPERIMENTAL

The oxygen-deficient phase $Sr_2MnO_{3.5}$ was prepared via standard solid-state reaction using a stoichiometric mixture of high-purity Mn_2O_3 and $SrCO_3$. A 2% excess of $SrCO_3$ was required to yield a single-phase sample. The powder sample was pressed into a pellet and heated in N_2 gas at 1350°C for 24 h, with one intermediate grinding. This "as-synthesized" sample was oxygen-deficient $Sr_2MnO_{3.64(1)}$ but this could be further reduced upon low-temperature annealing in a mixture of H_2/N_2 gas (10% H_2/90% N_2) at 550°C for 8 h. This produced the pure Mn^{3+} material, $Sr_2MnO_{3.5}$.

X-ray powder diffraction (XRPD) data were collected using a Siemens D5000 diffractometer (monochromated Cu$K\alpha_1$ radiation source, position sensitive detector, transmission mode). Neutron powder diffraction (NPD) patterns were recorded on the high-resolution powder diffraction diffractometer D2B at Institut Laue-Langevin, Grenoble (wavelength 1.594 Å, Ge monochromator). Rietveld structural refinements were carried out using the GSAS (16) package. Electron diffraction was performed with a Philips CM20 microscope. The magnetic susceptibility of the sample was measured using a Quantum Design SQUID Magnetometer. Both zero-field-cooled (ZFC) and field-cooled (FC) measurements were carried out under an applied field of 1 T. Thermogravimetric measurements were recorded on a Rheometric Scientific STA 1500 Simultaneous Thermal Analyser.

RESULTS AND DISCUSSION

Structural and magnetic data were collected on the sample with stoichiometry $Sr_2MnO_{3.64}$, since it proved difficult to obtain large homogeneous samples of $Sr_2MnO_{3.50}$ suitable for NPD studies. XRPD data were consistent with previous reports of the related oxygenated phase Sr_2MnO_4, which suggested the phase to be body-centered tetragonal, space group $I4/mmm$. The lattice parameters, $a = 3.81829(6)$ Å; $c = 12.58165(19)$ Å, showed an expansion in the c-parameter in agreement with the increase in the size of the Mn cations upon reduction from Mn^{4+} to Mn^{3+}. Rietveld structural refinement based on the XRPD data, converged with $\chi^2 = 4.441$ and reliability factors $R_p = 1.47\%$ and $R_{wp} = 2.12\%$. This revealed that the oxygen vacancies were located in the "MnO_2" planes but no superstructure reflections were observed in the XRPD pattern.

Magnetic susceptibility (χ) studies revealed a broad peak centered at ~ 280 K, Fig. 2. The transition is characteristic of AFM ordering in $n = 1$ layered materials. The $1/\chi$–T plot, Fig. 3, is linear above the transition in accordance with the Curie–Weiss Law with a paramagnetic moment of $6.34\,\mu_B$ per Mn and a Weiss constant $\theta = -718$ K. The paramagnetic moment per Mn is significantly higher than the expected spin-only value (Mn^{3+} $4.90\,\mu_B$, Mn^{4+} $3.87\,\mu_B$), and suggests the formation of some small superparamagnetic clusters. Similar behavior has been reported

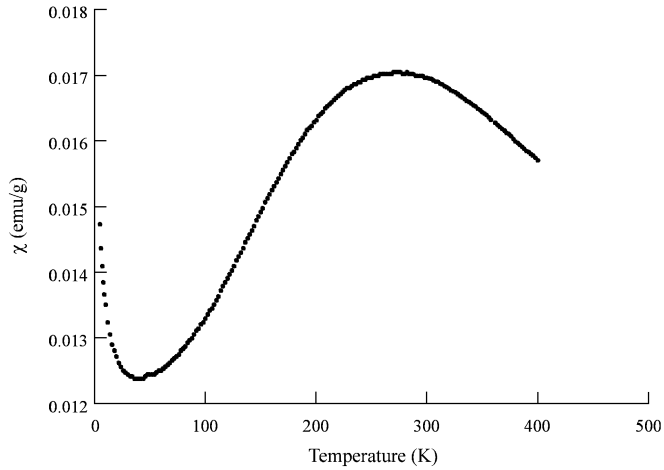

FIG. 2. Magnetic susceptibility of $Sr_2MnO_{3.5+x}$.

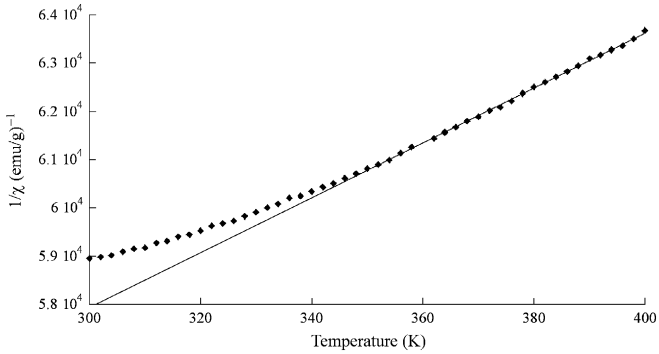

FIG. 3. Inverse magnetic susceptibility of $Sr_2MnO_{3.5+x}$.

in RP phases with competing FM and AFM interactions within the layers (17, 18), which may result from a mixed Mn^{3+}/Mn^{4+} oxidation state.

Neutron diffraction was used to examine the defect structure more thoroughly. All further refinements discussed were performed on NPD data. Rietveld structural refinement based on the 300 K data revealed that the space group $I4/mmm$ was unable to provide acceptable agreement between the observed and calculated profiles. In the NPD profile collected at 2 K, low-intensity additional peaks indicated the presence of magnetic ordering. However, these could be indexed only using a very large cell, which would be inconsistent with the magnetic ordering expected for a simple disordered model based on $I4/mmm$. A more complex structure was implied and crystallites were, therefore, subjected to an electron microscopy examination.

Electron diffraction (ED) studies clearly revealed a superstructure (Fig. 4) implying an ordering of the oxygen vacancies to give a primitive monoclinic cell with $a = 6.85$ Å; $b = 10.8$ Å; $c = 10.26$ Å; $\beta = 104.6°$. This space group was transformed to an equivalent cell with $a = 6.85$ Å; $b = 10.8$ Å; $c = 10.8$ Å; $\beta = 113.2°$ to assist the visualization of possible ordering schemes, since this cell is simply related to the body-centered tetragonal sub-cell vectors $(\boldsymbol{a_t}, \boldsymbol{b_t}, \boldsymbol{c_t})$ by $\boldsymbol{a} = \frac{1}{2}(-\boldsymbol{a_t} - \boldsymbol{b_t} + \boldsymbol{c_t})$, $\boldsymbol{b} = 2(-\boldsymbol{a_t} + \boldsymbol{b_t})$, $\boldsymbol{c} = 2(\boldsymbol{a_t} + \boldsymbol{b_t})$. The a_tb_t tetragonal plane, therefore, becomes the bc plane in the monoclinic supercell. Rietveld structure refinement based on various plausible distributions of the oxygen vacancies showed that only one arrangement appeared consistent with such a large unit-cell in the bc plane, ca. 10×10 Å. The arrangement, which corresponds to $P2_1/c$ symmetry, is similar to that seen for the ordered perovskite $SrMnO_{2.5}$ ($5.43 \times 10.86 \times 3.84$ Å; space group $Pbam$). The refinement gave a good fit using this model with a 36-point interpolated background and a pseudo-Voigt profile function, with reduced $\chi^2 = 4.228$, $R_{wp} = 4.44\%$, $R_p = 3.32\%$. For comparison purposes, the refinement using the tetragonal space group $I4/mmm$ resulted in $\chi^2 = 13.50$, $R_{wp} = 5.75\%$, $R_p = 8.02\%$.

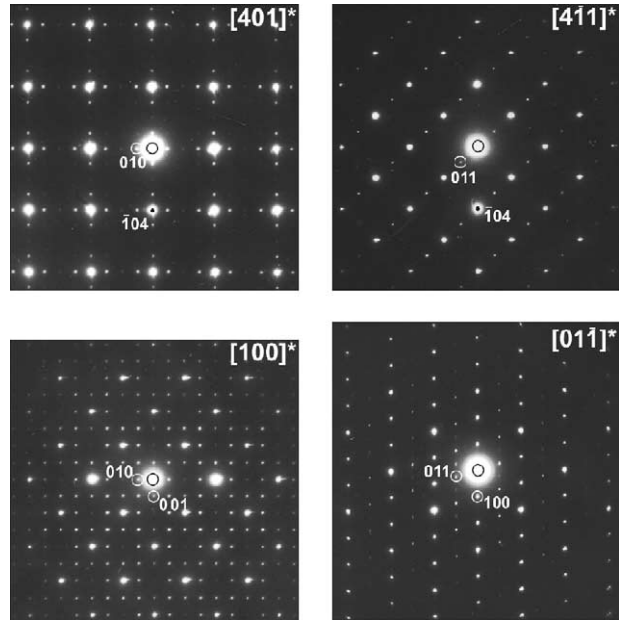

FIG. 4. Electron diffraction patterns of $Sr_2MnO_{3.5}$ along the zones [401]* (=[001]*$_t$), [100]* (=[$\bar{1}\bar{1}$1]*$_t$), [4$\bar{1}$1]* (=[$\bar{1}\bar{1}\bar{1}$]*$_t$) and [01$\bar{1}$]* (=[100]*$_t$). The superstructure reflections along the direction [$\bar{1}$04]* on the ED pattern of [401]* and along [$\bar{1}$22]* on the [01$\bar{1}$]* ED pattern belong to a different orientation variant and are introduced by twinning.

Hamilton reliability tests (19) confirmed that the improvement of fit on moving from $I4/mmm$ to $P2_1/c$ is statistically highly significant. Refined parameters and Mn–O bond lengths are given in Tables 1 and 2. Fractional occupancy of the O(4) site is consistent with a stoichiometry

TABLE 1
Refined Parameters of $Sr_2MnO_{3.5+x}$ at 300 K

Atom	x	y	z	U_{iso} * 100	Frac.
Sr(1)	0.290(1)	0.0003(10)	0.073(2)	1.2(1)	1
Sr(2)	0.299(1)	0.004(1)	0.575(1)	0.8(1)	1
Sr(3)	0.298(2)	0.243(1)	0.330(1)	1.3(2)	1
Sr(4)	0.292(2)	0.746(1)	0.316(1)	0.3(2)	1
Mn(1)	−0.006(2)	−0.002(1)	0.250(2)	0*	1
Mn(2)	−0.008(3)	0.257(2)	−0.0004(11)	0.3(1)	1
O(1)	−0.002(3)	0.140(1)	0.126(1)	1.7(2)	1
O(2)	0.003(3)	0.104(1)	0.397(1)	1.9(2)	1
O(3)	0.001(2)	0.129(1)	0.865(1)	0.9(2)	1
O(4)	0.002(1)	0.136(4)	0.634(5)	1.0*	0.23(1)
O(5)	0.308(2)	−0.012(2)	0.338(2)	2.0(3)	1
O(6)	0.309(2)	0.014(1)	0.821(2)	1.3(2)	1
O(7)	0.310(2)	0.252(1)	0.083(1)	0*	1
O(8)	0.317(2)	0.742(1)	0.068(1)	1.1(3)	1

Note. *denotes where thermal parameters were fixed—refer to text. All atoms in general *4e* position.

$a = 6.85238(28)$ Å; $b = 10.8131(4)$ Å; $c = 10.8068(4)$ Å; $\beta = 113.2472(35)°$.

Space group $P2_1/c$; $\chi^2 = 4.228$; $R_{wp} = 04.44\%$ and $R_p = 03.32\%$.

TABLE 2
Bond Lengths from NPD Data Collected at 300 K

(a) Mn–O bond lengths (Å)*			
Mn1–O1	2.05(2)	Mn2–O1	1.85(2)
Mn1–O2	1.94(2)	Mn2–O2	1.89(3)
Mn1–O3	1.85(2)	Mn2–O3	2.03(2)
Mn1–O5	1.99(2)	Mn2–O7	2.00(2)
Mn1–O6	1.92(2)	Mn2–O8	1.95(3)
O–Mn–O bond angles (deg)			
O1–Mn1–O2	95.2(1)	O1–Mn2–O3	93.9(1)
O1–Mn1–O3	96.3(1)	O1–Mn2–O7	87.1(1)
O1–Mn1–O5	93.6(8)	O1–Mn2–O8	88.7(1)
O1–Mn1–O6	94.6(8)	O2–Mn2–O3	95.7(6)
O2–Mn1–O5	87.8(9)	O2–Mn2–O7	90.9(1)
O2–Mn1–O6	92.8(1)	O2–Mn2–O8	92.7(1)
O3–Mn1–O5	88.7(8)	O3–Mn2–O7	89.6(8)
O3–Mn1–O6	89.1(9)	O3–Mn2–O8	94.9(1)

*The O(4) position is included but is only 20% occupied: Mn1–O4 = 1.91(5) Å; Mn2–O4 = 1.84(5) Å.

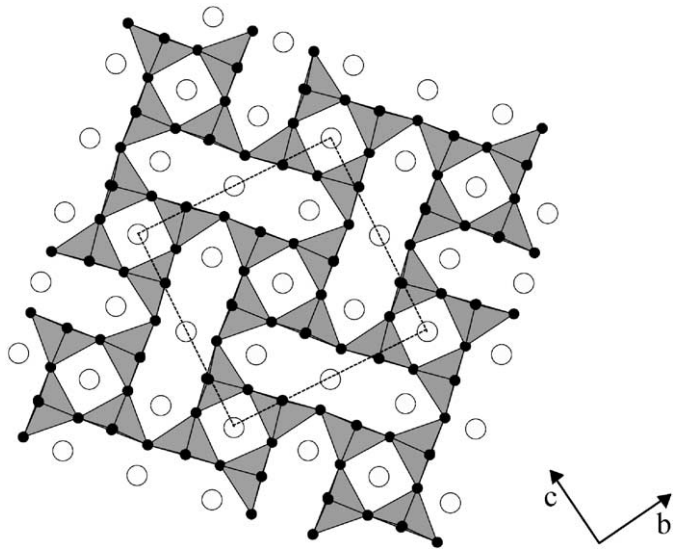

FIG. 6. Defect perovskite layer of $Sr_2MnO_{3.5}$.

$Sr_2MnO_{3.61}$, which is in excellent agreement with that deduced from TG analysis, $Sr_2MnO_{3.64}$. TG analysis of samples involved heating in a stream of O_2 at 400°C to form the pure Mn^{4+} material, Sr_2MnO_4. In addition, full decomposition was also carried out in a mixture of 10% H_2/90% N_2 at 1000°C to form SrO and MnO. To avoid correlation effects, the temperature factor for O(4) was fixed at a sensible value. The temperature factors for two atoms were slightly negative and were therefore constrained to zero. Figures 5 and 6 show the relationship between the tetragonal and monoclinic sub-cells and the defect structure of the layers in the stoichiometric $Sr_2MnO_{3.5}$. Although similar to $SrMnO_{2.5}$ (compare Figs. 1 and 6), the structure consists of elongated pseudo-hexagonal channels in the layers. This is the first-known example of a structure of this type. Due to the broad nature of the maximum in the magnetic susceptibility plot, it is possible that the 300 K NPD data contain a very small magnetic contribution. Given the weak intensity of the magnetic reflections at 2 K, as described below, the presence of magnetic effects was considered to be fairly insignificant, but could possibly have a small effect on the thermal parameters.

Data collected at 2 K show the appearance of small low angle peaks, attributed to the AFM ordering of the phase. Although most of these additional peaks could be indexed on the nuclear monoclinic cell, no simple AFM structure could account for the intensities of these peaks. A magnetic model was therefore sought using the Kanamori–Goodenough rules (20) to predict the dominant exchange interactions. The Mn^{3+} ions have the electronic configuration $t_{2g}^3 e_g(dz^2)^1$, and the magnetic exchange between adjacent square-based pyramids can be ascertained by the interactions between the singly occupied dz^2 orbitals, and the perpendicular, empty $dx^2 - y^2$ orbitals. This leads to the prediction of FM exchange when a connecting oxygen anion links a dz^2 orbital with a vacant dx^2-y^2 orbital, and

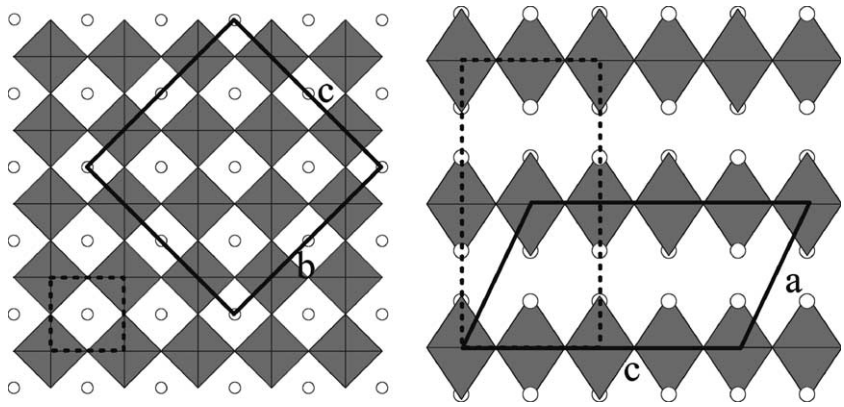

FIG. 5. Relationship between *I*4/*mmm* sub-cell and monoclinic unit-cell, where *b* is the unique axis.

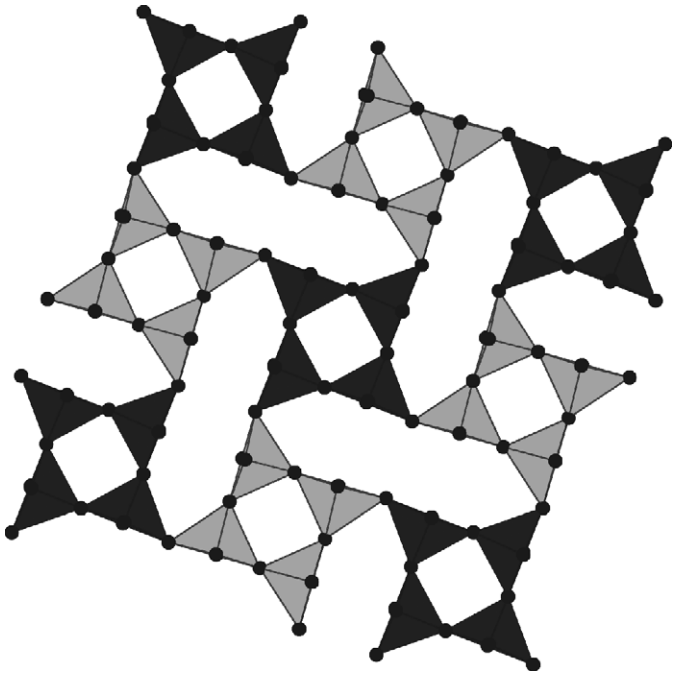

FIG. 7. Magnetic structure of $Sr_2MnO_{3.5}$. Spin-up polyhedra in gray; spin-down polyhedra in black.

an AFM alignment upon interaction of two dz^2 orbitals. Hence, the intralayer magnetic structure was deduced as clusters of four ferromagnetically aligned moments, which are arranged antiferromagnetically to other clusters within the perovskite block layers, as shown in Fig. 7.

Some of the magnetic peaks required doubling of the nuclear unit-cell along [100] implying a predominantly AFM interlayer exchange interaction. The most intense peak which indicated doubling along the *a*-axis was the $[\frac{1}{2}, 1, 0]$ at $2\theta \sim 11.2^\circ$. The intralayer magnetic structure shown in Fig. 7 with AFM order between the layers in the [100]-direction provided a very good fit to the magnetic NPD observations. However, it was clear that the magnetic moments are not simply aligned along the axis perpendicular to the Mn–O layers, as is normal in tetragonal $n = 1$ RP phases. The low intensity of the magnetic peaks introduces some uncertainty as to the precise magnetic order, but the best agreement was achieved with a tilting of the moments in adjacent layers as shown in Fig. 8. The refined Mn magnetic moment is 2.8(1) μ_B and is directed at an angle of 27(3)° to an axis perpendicular to the layers. This direction is close to the monoclinic *a*-axis. The magnetic structure can be attributed to the unique intralayer order, and may be rationalized by the existence of competing interlayer interactions, which cannot be satisfied by a simple co-linear arrangement. The Rietveld plot is shown in Fig. 9 and refined parameters and Mn–O bond lengths are given in Tables 3 and 4. The refinement converged to $\chi^2 = 5.237$ with reliability factors $R_p = 3.76\%$ and $R_{wp} = 4.97\%$. Some of the metal ion temperature factors were fixed at zero since they adopted slightly negative values when unconstrained; the partially occupied O(4) site was fixed at a reasonable value, as for the 300 K refinement. The implied stoichiometry, $Sr_2MnO_{3.60}$, again agrees well with the analytical value. Although the χ^2 values for the refinements are slightly higher than are sometimes achieved, they are considered acceptable for such a complex structure using a model which clearly represents only an average structure owing to the partial occupation of the O(4) site.

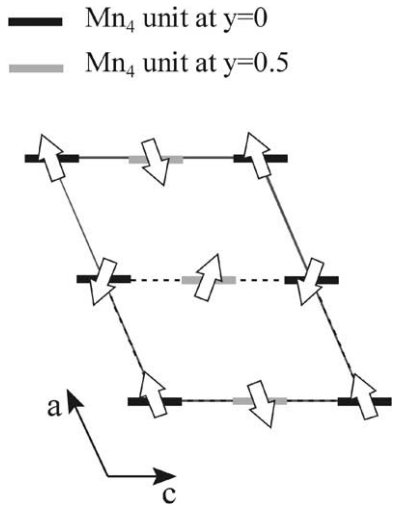

FIG. 8. Tilting of the Mn moments in the *ac* plane.

TABLE 3
Refined Parameters of $Sr_2MnO_{3.5+x}$ at 2 K

Atom	*x*	*y*	*z*	U_{iso} * 100	Frac.
Sr(1)	0.289(1)	0.001(1)	0.074(1)	0.1(1)	1
Sr(2)	0.300(1)	0.003(1)	0.577(1)	0*	1
Sr(3)	0.295(3)	0.243(1)	0.333(1)	1.2(2)	1
Sr(4)	0.292(2)	0.747(1)	0.314(1)	0.5(2)	1
Mn(1)	−0.006(2)	0.000(1)	0.250(2)	0*	1
Mn(2)	−0.005(4)	0.256(2)	−0.001(1)	0*	1
O(1)	−0.001(2)	0.139(1)	0.126(1)	1.3(2)	1
O(2)	−0.001(3)	0.106(1)	0.394(1)	1.1(2)	1
O(3)	0.004(3)	0.128(1)	0.866(1)	1.0(2)	1
O(4)	−0.0046*	0.1294*	0.6293*	1.0*	0.21(1)
O(5)	0.307(1)	−0.011(1)	0.336(2)	0.9(2)	1
O(6)	0.310(1)	0.015(1)	0.824(2)	0.5(2)	1
O(7)	0.312(2)	0.254(1)	0.085(1)	0.1(2)	1
O(8)	0.317(2)	0.742(1)	0.067(1)	0.9(3)	1

Note. *denotes unrefined and fixed variables—refer to text. All atoms in general *4e* position.

$a = 6.84057(30)$ Å; $b = 10.77945(43)$ Å; $c = 10.77423(42)$ Å; $\beta = 113.211(4)$.

Space-group: $P2_1/c$; $\chi^2 = 5.273$; $R_{wp} = 4.97\%$ and $R_p = 3.76\%$.

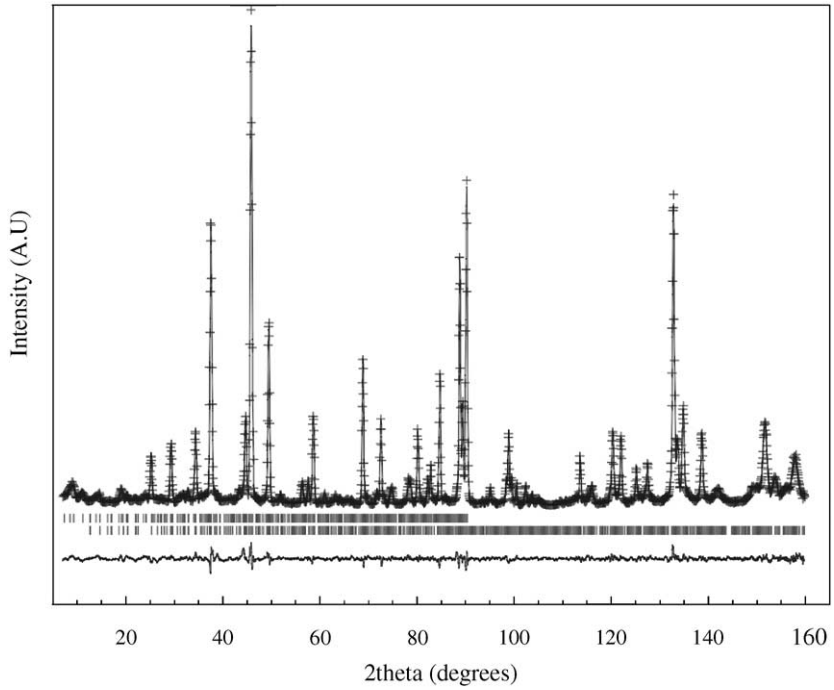

FIG. 9. Rietveld profile of neutron powder diffraction data for $Sr_2MnO_{3.5+x}$ at 2 K. The vertical ticks show the reflection positions: magnetic (upper) and nuclear (lower). The strongest magnetic reflections occur below $2\theta = 23^\circ$.

SUMMARY

The single-layered phase $Sr_2MnO_{3.5}$ crystallizes with the oxygen vacancies forming an ordered array in the "MnO_2" layers of the perovskite block. Although the defect structure formed can be compared with that found in the oxygen-deficient perovskite $SrMnO_{2.5}$ and the analogous $Ca_2MnO_{3.5}$, the vacancies order to give a new type of structure of corner connected Jahn–Teller distorted MnO_5 square-based pyramids. $Sr_2MnO_{3.5}$ orders antiferromagnetically below 280 K and the magnetic structure contains FM clusters aligned antiferromagnetically to each other within the perovskite block layers.

TABLE 4
Bond Lengths from NPD Data Collected at 2 K

(a) Mn–O bond lengths (Å)*			
Mn1–O1	2.02(2)	Mn2–O1	1.85(2)
Mn1–O2	1.91(3)	Mn2–O2	1.88(2)
Mn1–O3	1.87(2)	Mn2–O3	2.01(2)
Mn1–O5	1.98(2)	Mn2–O7	1.99(3)
Mn1–O6	1.92(1)	Mn2–O8	1.96(3)
(b) O–Mn–O bond angles (deg)			
O1–Mn1–O2	95.4(7)	O1–Mn2–O3	93.9(1)
O1–Mn1–O3	95.8(1)	O1–Mn2–O7	87.3(9)
O1–Mn1–O5	93.0(8)	O1–Mn2–O8	88.7(1)
O1–Mn1–O6	94.8(8)	O2–Mn2–O3	95.7(6)
O2–Mn1–O5	89.3(1)	O2–Mn2–O7	90.9(1)
O2–Mn1–O6	93.5(1)	O2–Mn2–O8	92.7(1)
O3–Mn1–O5	88.6(9)	O3–Mn2–O7	89.6(8)
O3–Mn1–O6	87.3(9)	O3–Mn2–O8	94.9(1)

*The O(4) position is included but is only 20% occupied: Mn1–O4 = 1.89(2) Å; Mn2–O4 = 1.87(2) Å.

ACKNOWLEDGMENTS

We thank EPSRC and IUAP 4 for financial support, and EPSRC for a studentship (L.J.G.) and the provision of NPD facilities. We also thank Alan Hewat and Peter Cook for assistance in obtaining NPD data and to Quantum Design for magnetic susceptibility measurements.

REFERENCES

1. A. P. Ramirez, *J. Phys.: Condens. Matter* **9,** 8171 (1997).
2. Y. Moritomo, Y. Tomioka, A. Asamitsu, and Y. Tokura, *Nature (London)* **380,** 141 (1996).
3. R. Mahesh, R. Mahendiran, A. K. Raychaudhuri, and C. N. R. Rao, *J. Solid State Chem.* **122,** 448 (1996).
4. S. N. Ruddlesden and P. Popper, *Acta Crystallogr.* **11,** 54 (1958).
5. N. Mizutani, A. Kitazawa, N. Onkuma, and M. Kato, *Kogyo Kaguka Zasshi* **73**(6), 1087 (1971).

6. D. Balz and K. Plieth, *Z. Elektrochem.* **59,** 545 (1955).
7. R. Kriegel, H. Borrmann, A. Simon, and A. Feltz, *Z Naturforsch.* **48b,** 15 (1993).
8. R. Kriegel and A. Feltz, *Z. Anorg. Allg. Chem.* **617,** 99 (1992).
9. J.-C. Bouloux, J.-L. Soubeyroux, G. Le Flem, and P. Hagenmuller, *J. Solid State Chem.* **38,** 34 (1998).
10. D. E. Cox, G. Shirane, R. J. Birgeneau, and J. B. MacChesney, *Phys. Rev.* **188**(2), 930 (1969).
11. J. F. Mitchell, J. E. Millburn, M. Medarde, S. Short, and J. D. Jorgensen, *J. Solid State Chem.* **141,** 599 (1998).
12. M. E. Leonowicz, K. R. Poeppelmeier, and J. M. Longo, *J. Solid State Chem.* **59,** 71 (1985).
13. V. Caignaert, *J.Magn. Magn. Mater.* **166,** 117 (1997).
14. V. Caignaert, N. Nguyen, A. Ducouret, M. Hervieu, and B. Raveau, *Mater. Res. Bull.* **20,** 479 (1985).
15. K. R. Poeppelmeier, M. E. Leonowicz, J. C. Scanlon, J. M. Longo, and W. B. Yelon, *J. Solid State Chem.* **45,** 71 (1982).
16. A. C. Larson and R. B. Von Dreele, "General Structure Analysis System." Los Alamos National Laboratory, Los Alamos, NM, 1994.
17. R. K. Li and C. Greaves, *J. Solid State Chem.* **153,** 34 (2000).
18. S. Ghosh and P. Adler, *Solid State Commun.* **116,** 585 (2000).
19. W. C. Hamilton, *Acta Crystallogr.* **18,** 502 (1965).
20. J. B. Goodenough, "Magnetism and the Chemical Bond." Robert E. Krieger Publishing Company, Huntington, New York, 1976.